Downstream Weather Impacts Associated with Atmospheric Blocking over the Northeast Pacific

M. L. CARRERA, R. W. HIGGINS, AND V. E. KOUSKY

NOAA/NWS/NCEP Climate Prediction Center, Camp Springs, Maryland

(Manuscript received 9 December 2003, in final form 17 June 2004)

ABSTRACT

Relationships between atmospheric blocking over the Alaskan region of the northeast Pacific, referred to as Alaskan blocking, and weather extremes over North America during boreal winter 1979–2000 are examined. A total of 37 atmospheric blocking events are identified with durations ranging from 8 to 25 days and a mean duration of 11.3 days. A total of 15.6% of the days during the boreal winter belonged to an Alaskan blocking event.

The number of blocked days over the Alaskan region was found to be sensitive to the phase of the ENSO cycle with a reduced (increased) number of blocked days during El Niño (La Niña/neutral) winters. The average number of blocked days during El Niño winters was 12, compared with 31.2 and 27 for neutral and La Niña winters, respectively. The mature Alaskan block possesses characteristics, which are typical of blocking episodes, including the equivalent barotropic structure of the blocking anticyclone, the meridional flow both upstream and downstream of the block, the equatorward shift of the Pacific storm track, downstream development of 500-hPa geopotential height, and sea level pressure anomalies over North America.

The surface temperature analysis revealed a significant shift in the daily mean surface temperature distribution during Alaskan blocking toward colder temperatures in the region extending from the Yukon southeastward to the southern plains of the United States, associated with a reduced variance of surface temperatures. Over extreme western Alaska there is a shift in the daily mean surface temperature distribution toward warmer temperatures. The shift toward colder (warmer) daily mean surface temperatures is also accompanied by a shift in the tails of the distribution toward more extreme cold (warm) days in these two regions. During Alaskan blocking, the regions of southern California, the Southwest, and the Intermountain West all possess a higher frequency of heavy precipitation days when compared with the long-term winter climatology. Over the eastern half of the United States, the Ohio Valley and the southeast regions experience a greater percentage of heavy precipitation days during Alaskan blocking.

1. Introduction

Episodes of prolonged extreme weather conditions, such as droughts and floods (Trenberth and Guillemot 1996; Mo et al. 1997), and heat waves (Kalkstein et al. 1996; Karl and Knight 1997), are of considerable importance to society. It is now widely recognized that such weather extremes are often associated with recurrent atmospheric flow anomalies (Dole 1986a,b; Higgins and Schubert 1994, 1996; Robertson and Ghil 1999) that can last from several days up to a few weeks.

One feature that is often implicated in these events is the persistent anticyclonic flow anomaly, which is often referred to as an atmospheric ''blocking'' episode (Dole 1986a,b; Higgins and Schubert 1996; Higgins and Mo 1997). Atmospheric blocking refers to the situation where the normal zonal flow is interrupted by strong and persistent meridional flow (Rex 1950a,b). The normal eastward progression of synoptic disturbances is obstructed, as the systems are forced to the north and south of the blocking anticyclone, leading to anomalous storm tracks (Nakamura and Wallace 1990).

Numerous studies have alluded to the inherent problems of numerical weather prediction models in forecasting events of atmospheric blocking (Tibaldi and Molteni 1990; Anderson 1993; Tibaldi et al. 1994; Chen and Van den Dool 1995; D'Andrea et al. 1998). Chen and Van den Dool (1995) noted that the poor forecast skill beyond a few days results principally from the inability of numerical weather prediction models to simulate the onset and evolution of blocking flows. A finding common to most studies is that medium-range forecast models underestimate the observed blocking frequency owing to their inherent problems in transitioning to a blocked state. However, Tibaldi and Molteni (1990) and Tibaldi et al. (1994) demonstrated that numerical models perform measurably better in maintaining a blocked flow once the signature of the atmospheric

Corresponding author address: Dr. M. L. Carrera, RSIS/Climate Prediction Center, NOAA/NWS/NCEP, Rm. 605, 5200 Auth Rd., Camp Springs, MD 20746.
E-mail: Marco.Carrera@noaa.gov

block is present in the initial conditions. Recently, with the introduction of ensemble forecasting systems at both the National Centers for Environmental Prediction (NCEP) and at the European Centre for Medium-Range Weather Forecasts (ECMWF), the forecasting of atmospheric blocking at the medium ranges has improved (Watson and Colucci 2002; Pelly and Hoskins 2003b).

The region of the North Pacific has been identified as a preferred region for atmospheric blocking during the boreal winter season (Elliott and Smith 1949; Rex 1950b; Dole and Gordon 1983; Dole 1986a,b; Tibaldi and Molteni 1990; Tibaldi et al. 1994; Renwick and Wallace 1996; Higgins and Schubert 1996; Pelly and Hoskins 2003a,b). Robertson and Ghil (1999) classified weather regimes over the North Pacific sector and identified positive 700-hPa geopotential height anomalies over Alaska as one of six principal weather patterns dominating the boreal winter season. A similar classification of flow regimes over the Pacific–North American sector identified ''Pacific blocking,'' characterized by a high-amplitude ridge over the Gulf of Alaska and a trough over the western United States, as the second most commonly occurring 500-hPa flow regime for the six winter periods from 1987/88 to 1992/93 (Stoss and Mullen 1995).

The presence of persistent positive height anomalies in the vicinity of Alaska has been linked to heavy precipitation over California and the southwestern United States. A study by Ely et al. (1994) found that positive 700-hPa height anomalies situated over Alaska, poleward of a low pressure anomaly off the west coast of California, was the dominant circulation pattern contributing to anomalous moisture transport and heavy winter flooding over the southwestern United States. Robertson and Ghil (1999) also found heavy precipitation in the southwest United States to be preferentially associated with Alaskan ridging, noting further that this Alaskan ridging also favored more extreme cold days in western Washington State and the southwest.

Extratropical low-frequency variability, and specifically how this variability changes as a function of the ENSO cycle, has been the subject of several studies (Mullen 1989; Renwick and Wallace 1996; Chen and Van den Dool 1997; Renwick 1998; Chen and Van den Dool 1999; Compo et al. 2001). Mullen (1989) investigated the impact of Pacific sea surface temperatures (SST) upon blocking in the Northern Hemisphere by means of a series of sensitivity experiments with a general circulation model. He found that changes in the Pacific SSTs acted principally to shift the preferred locations for atmospheric blocking, but did not strongly affect the dynamics or persistence of individual blocking events. The combination of a warm tropical SST anomaly and a cool extratropical SST anomaly over the Pacific, as is found during El Niño events (Lau 1997), acted to shift North Pacific blocking activity eastward from the Aleutian Islands toward the west coast of North America (Mullen 1989).

The strong impact of tropical Pacific SSTs upon blocking was also noted in a study by Chen and Van den Dool (1997). They noted that in the region between 180° and 140°W in the North Pacific blocking frequencies increased from 10% during El Niño winters to 15% during La Niña winters. Renwick and Wallace (1996) attributed the increased frequency of blocking in the Alaskan region of the North Pacific during the cool phase of ENSO to the combined effects of a higher mean and larger variance of the 500-hPa geopotential heights. A recent study by Compo et al. (2001) drew similar conclusions as Renwick and Wallace (1996).

The objective of this study is to examine the relationship between blocking in the Alaskan region of the North Pacific, termed Alaskan blocking, and weather extremes downstream over North America during the boreal cold season. Alaskan blocking can be regarded as one flow regime, and we are interested in investigating the changes to the statistical distributions of temperature and precipitation during the Alaskan blocking regime as compared to the long-term winter climatology. Are extremes of surface temperature and precipitation more likely to occur during the Alaskan blocking regime? Results from this study are intended to aid forecasters with extended-range outlooks.

The datasets and methodology used to identify blocking events are given in section 2. Interannual variability of Alaskan blocking is considered in section 3. The structure and evolution of the composite Alaskan blocking event is described in section 4 with emphasis on precursors and anomalies during the blocking events. Changes in daily mean surface temperature and precipitation distributions during blocking episodes are discussed in section 5. A summary and conclusions are given in section 6.

2. Data and methodology

The NCEP–National Center for Atmospheric Research (NCAR) reanalysis (Kalnay et al. 1996; hereafter referred to as the NCEP reanalysis) daily averaged 500-hPa geopotential heights for the 22-yr period 1979–2000 are used to identify events of atmospheric blocking. Following the recent article by Kistler et al. (2001), which concluded that the reanalysis climatology after 1979 was the most reliable, owing to the introduction of satellite data, we restrict the analysis to the period from 1979 onward.

A global gridded daily maximum and minimum surface temperature dataset over land at 2.5° latitude–longitude resolution is used to document the temperature impacts associated with the Alaskan blocking regime. The data begin in 1979 and are derived from ''first order'' World Meteorological Organization (WMO) meteorological recording stations received over the Global Telecommunication System (GTS), with typically between 6000–7000 stations reporting daily, including roughly 950 stations over the North American region

(15°–90°N, 60°–170°W) (P. Xie 2002, personal communication). The interpolation procedure used to grid the station data is the same as that used in Xie et al. (1996). [The data can be obtained by contacting Dr. Xie at the Climate Prediction Center (CPC)]. Daily mean surface temperatures were calculated by averaging the daily maximum and minimum temperatures at each grid point.

Precipitation impacts are assessed via a U.S.–Mexico merged historical daily precipitation analysis. The dataset is at a horizontal resolution of 1° latitude–longitude and is derived from rain gauge measurements for the entire study period (1979–2000). Extensive quality control measures have been applied to the data as discussed in Higgins et al. (2000b), [The Higgins et al. (2000b) reference can be found at the CPC Web site (http://www.cpc.ncep.noaa.gov/research_papers/ncep_cpc_atlas/7/index.html), including information on how to access the data.] Mo and Berbery (2004), and Mo and Juang (2003) have used this dataset in their studies of summer precipitation regimes over North America.

To identify blocking events over the Alaskan region of the northeast Pacific we use the threshold crossing procedure of Dole and Gordon (1983) applied to the 500-hPa geopotential height anomaly field. This procedure has been used in several previous studies related to persistent anticyclonic anomalies and blocking (Higgins and Schubert 1996; Renwick and Wallace 1996; Black 1997; Higgins and Mo 1997; Renwick 1998; Black and Evans 1998). For this study, the threshold and duration criteria chosen were 100 m and 8 days. The duration criteria of 8 days is shorter than the 10 days typically found in previous studies (Dole and Gordon 1983; Higgins and Schubert 1996; Higgins and Mo 1997), but was used to increase the sample size of atmospheric blocking events.

Prior to applying the threshold crossing procedure, the 500-hPa geopotential height anomaly fields were calculated by first removing the local seasonal cycle, defined as the mean plus the annual and semiannual harmonics of the 22-yr (1979–2000) mean annual cycle, and then applying a 10-day low-pass Lanczos filter with 121 weights (Duchon 1979). Note that defining the local seasonal cycle as the mean plus the first four harmonics gave the identical set of blocking events. A blocked day is defined as any day in which the 500-hPa geopotential height anomaly exceeds 100 m at the ''key point.'' A blocking event occurs when the 500-hPa geopotential height anomaly exceeds 100 m at the key point for at least 8 consecutive days.

The key point chosen in the northeast Pacific is located at 62.5°N and 162.5°W, centered over extreme western Alaska. A plot of the geographical distribution of the total number of persistent positive 500-hPa geopotential height anomaly events (i.e., blocking events) satisfying the selection criteria of (100 m, 8 days) for the December–January–February–March (DJFM) period from 1979 to 2000 (not shown) revealed this location as a local maximum. Renwick and Wallace (1996) chose this same region to examine the interannual variability of atmospheric blocking, noting that the circulation pattern associated with Alaskan blocking had the largest medium-range rms errors in the ECMWF model.

TABLE 1. Summary of atmospheric blocking events for the key point located at 62.5°N, 162.5°W in the northeast Pacific. The onset and end times for each event are given along with the duration in days.

Event No.	Onset date	End date	Duration (days)
1	18 Feb 1979	26 Feb 1979	9
2	22 Mar 1979	2 Apr 1979	12
3	3 Jan 1980	10 Jan 1980	8
4	23 Jan 1980	30 Jan 1980	8
5	11 Feb 1980	18 Feb 1980	8
6	18 Dec 1980	25 Dec 1980	8
7	4 Feb 1981	11 Feb 1981	8
8	1 Feb 1982	12 Feb 1982	12
9	22 Feb 1982	5 Mar 1982	12
10	16 Dec 1983	29 Dec 1983	14
11	13 Jan 1984	20 Jan 1984	8
12	15 Dec 1984	30 Dec 1984	16
13	26 Jan 1985	10 Feb 1985	16
14	9 Feb 1986	20 Feb 1986	12
15	29 Dec 1987	6 Jan 1988	9
16	27 Jan 1988	4 Feb 1988	9
17	31 Jan 1989	19 Feb 1989	20
18	24 Feb 1989	17 Mar 1989	22
19	16 Mar 1990	26 Mar 1990	11
20	16 Dec 1990	9 Jan 1991	25
21	22 Jan 1991	29 Jan 1991	8
22	25 Feb 1991	4 Mar 1991	8
23	23 Dec 1992	11 Jan 1993	20
24	12 Feb 1993	22 Feb 1993	11
25	29 Jan 1994	5 Feb 1994	8
26	17 Feb 1994	25 Feb 1994	9
27	9 Feb 1995	16 Feb 1995	8
28	26 Feb 1995	9 Mar 1995	12
29	24 Jan 1996	2 Feb 1996	10
30	27 Feb 1996	8 Mar 1996	11
31	25 Mar 1996	1 Apr 1996	8
32	17 Dec 1996	30 Dec 1996	14
33	10 Mar 1997	17 Mar 1997	8
34	3 Jan 1998	11 Jan 1998	9
35	2 Mar 1998	9 Mar 1998	8
36	17 Dec 1998	26 Dec 1998	10
37	7 Feb 2000	14 Feb 2000	8
	Mean duration (days)		11.3

We restricted our analysis to those blocking events with onset times, that is, the time when the 500-hPa geopotential height anomaly first crosses the threshold of 100 m, in DJFM. The periods of January–March 1979 and December 2000 were also included. A buffer period was added at the end of March to allow for blocking events that continue into early April. The procedure yields a total of 37 blocking events (Table 1). A total of 417 out of the 2668 days, or 15.6%, belonged to blocking events. The blocking events have durations ranging from 8 to 25 days with a mean duration of 11.3 days. Each of the events is well separated by at least 10 days except for events 17 and 18 (see Table 1), which are separated by only 5 days. An examination of the

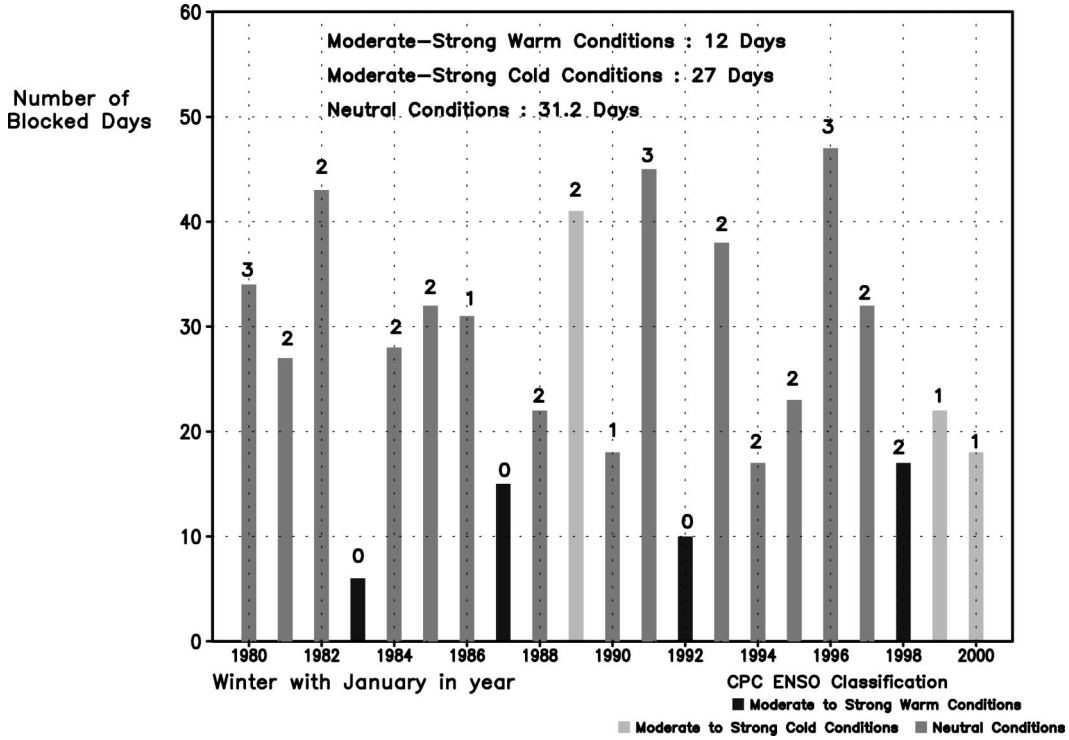

FIG. 1. Number of blocked days at 62.5°N, 162.5°W for each DJFM season. A blocked day is defined as any day in which the 500-hPa geopotential height anomaly (as defined in section 2) exceeds 100 m. The CPC ENSO classification has been used to classify each DJFM season. El Niño winters are given in dark gray, La Niña in light gray, and neutral in medium gray. The number of blocking events in the given DJFM season is given at the top of each bar. The average number of blocked days for El Niño (moderate–strong warm conditions), La Niña (moderate–strong cold conditions), and neutral winters is shown at the top of the figure.

individual synoptic maps for the time period between events 17 and 18 indicates that these are separate blocking episodes.

3. Interannual variability of Alaskan blocking

The interannual variability of Alaskan blocking, given by the total number of blocked days for each DJFM season from 1979/80 to 1999/2000, is shown in Fig. 1. Recall that a blocked day is defined as any day in which the 500-hPa geopotential height anomaly (as defined in section 2) exceeds 100 m at the key point of 62.5°N, 162.5°W located over extreme western Alaska. The number of blocked days will in general be different (larger) than the number of days belonging to blocking events owing to the fact that a string of blocked days may be shorter than 8 days, the minimum duration required to define a blocking event (see section 2). Each DJFM season is classified by ENSO phase. The classification is based upon the pattern and magnitude of SST anomalies in the tropical Pacific and can be found online (http://www.cpc.ncep.noaa.gov/research_papers/ncep_cpc_atlas/8/ensoyrs.txt). Each DJFM season is classified as warm, cold or neutral, with the warm and cold categories further subdivided into weak, moderate, and strong. For the purposes of this study, El Niño (La Niña) DJFMs are defined as moderate and strong warm (cold) events, and neutral DJFMs are featured in the remaining years. Higgins et al. (2002) utilized this same index and noted that it is identical to the Niño-3.4 index classification of ENSO for the boreal winter season. Of the 21 DJFM seasons considered, there are 4 El Niño winters (1982/83, 1986/87, 1991/92, and 1997/98), 3 La Niña winters (1988/89, 1998/99, and 1999/2000), and 14 neutral winters. The El Niño and La Niña events are consistent with those identified by Renwick and Wallace (1996) and Compo et al. (2001).

El Niño winters are associated with a much lower number of blocked days than either neutral or La Niña winters (Fig. 1). The average number of blocked days during El Niño winters is 12, compared with 31.2 and 27 for neutral and La Niña winters, respectively (see top of Fig. 1). Despite the small sample size, the difference in the mean number of blocked days between El Niño winters and neutral winters is statistically significant at the 99% level based upon a Student's *t* test for the difference of means (Hogg and Tanis 1988). The analysis is not sensitive to the key point of 62.5°N, 162.5°W as the eight surrounding grid points also show a preference for a reduced number of blocked days during El Niño winters as compared to either neutral or La Niña winters. Above each of the bars we show the num-

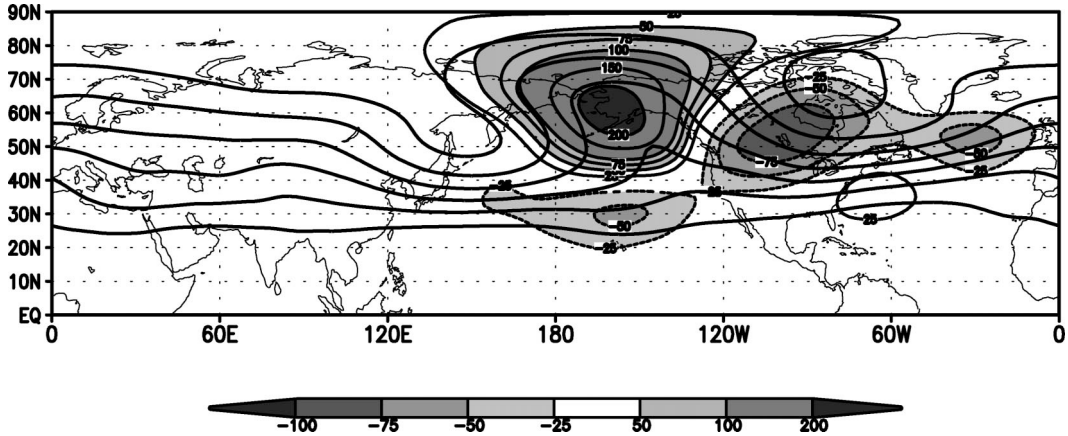

FIG. 2. Time-averaged 500-hPa geopotential height (contours) and anomalies (shaded) averaged over the duration of all 37 Alaskan blocking events. (Units: m.) Solid (dashed) contours represent positive (negative) anomalies.

ber of blocking events for each DJFM season. The total is 35 instead of 37 owing to the fact that the events in February and March of 1979 (events 1 and 2 in Table 1) are not shown. It is important to note that for the first three El Niño winters (1982/83, 1986/87, and 1991/92) there were no Alaskan blocking events.

4. Composite structure and evolution

In this section we document the structure and temporal evolution of Alaskan blocking events using composites. Emphasis is placed on precursors and significant circulation anomalies during Alaskan blocking events.

a. 500-hPa geopotential height

The 500-hPa geopotential height and anomalies, averaged over the duration of the 37 Alaskan blocking events, are shown in Fig. 2. Anomalies are calculated by removing the mean plus the first four harmonics of the 22-yr (1979–2000) mean annual cycle. The time-averaged circulation is dominated by positive 500-hPa geopotential height anomalies in excess of 230 m over western Alaska. As is typical of classic blocking situations, pronounced geostrophic meridional flow is present both upstream and downstream of the blocking ridge (Rex 1950a,b), with a distinct equatorward shift of the main westerly flow in the subtropical North Pacific. The splitting of the midlatitude flow extends over approximately 60° of longitude (180°–120°W). There is also evidence of downstream development with a large-scale trough over the North American continent and ridging off the U.S. southeast coast.

The temporal evolution of the 500-hPa geopotential heights and anomalies prior to the onset of the composite Alaskan blocking event are shown in Fig. 3. The plots represent time-lagged composites over all 37 blocking events keyed to the onset time (T0; Fig. 3f), defined as the first day in which the 500-hPa geopotential height anomaly crosses 100 m at the key point (62.5°N, 162.5°W) (see Table 1). A two-sided Student's *t* test (Hogg and Tanis 1988) was used to assess the statistical significance of the 500-hPa geopotential height anomalies. Several days prior to onset (Figs. 3a–c) a pronounced trough is observed upstream of Alaska with negative height anomalies over the Alaskan region. A similar result was noted by Higgins and Mo (1997) in their study of persistent North Pacific circulation anomalies. The trough in the North Pacific deepens, while the high-amplitude ridging associated with the block strengthens and retrogrades from the west coast of North America into the key region by day T − 1 (Figs. 3c–e). On or around day T + 2 (Fig. 3h) the mature block is clearly evident with characteristics similar to the time-averaged flow shown in Fig. 2, including the equatorward trough in the subtropical North Pacific and the pronounced trough downstream over North America.

The temporal evolution of the flow keyed to the decay of Alaskan blocks is shown in Fig. 4. Here T0 denotes the decay time (i.e., the time when the 500-hPa geopotential height anomaly falls below the 100-m threshold at the key point). At T − 3, 3 days prior to Alaskan blocking decay (Fig. 4c), the 500-hPa geopotential heights and anomalies look similar to those at T + 2 after the onset time (Fig. 3h) consistent with a rapid onset and decay of the blocks, as noted in previous studies (e.g., Dole 1989). The decay phase involves retrogression of the main positive and negative anomaly centers northwestward toward the northwest Pacific. At T + 4 (Fig. 4j) a deep trough occupies the key region over western Alaska.

b. Sea level pressure and vertically integrated moisture transport

Figures 5 and 6 are similar to Figs. 3 and 4, except that they show the composite sea level pressure (SLP) and vertically integrated moisture transport anomalies

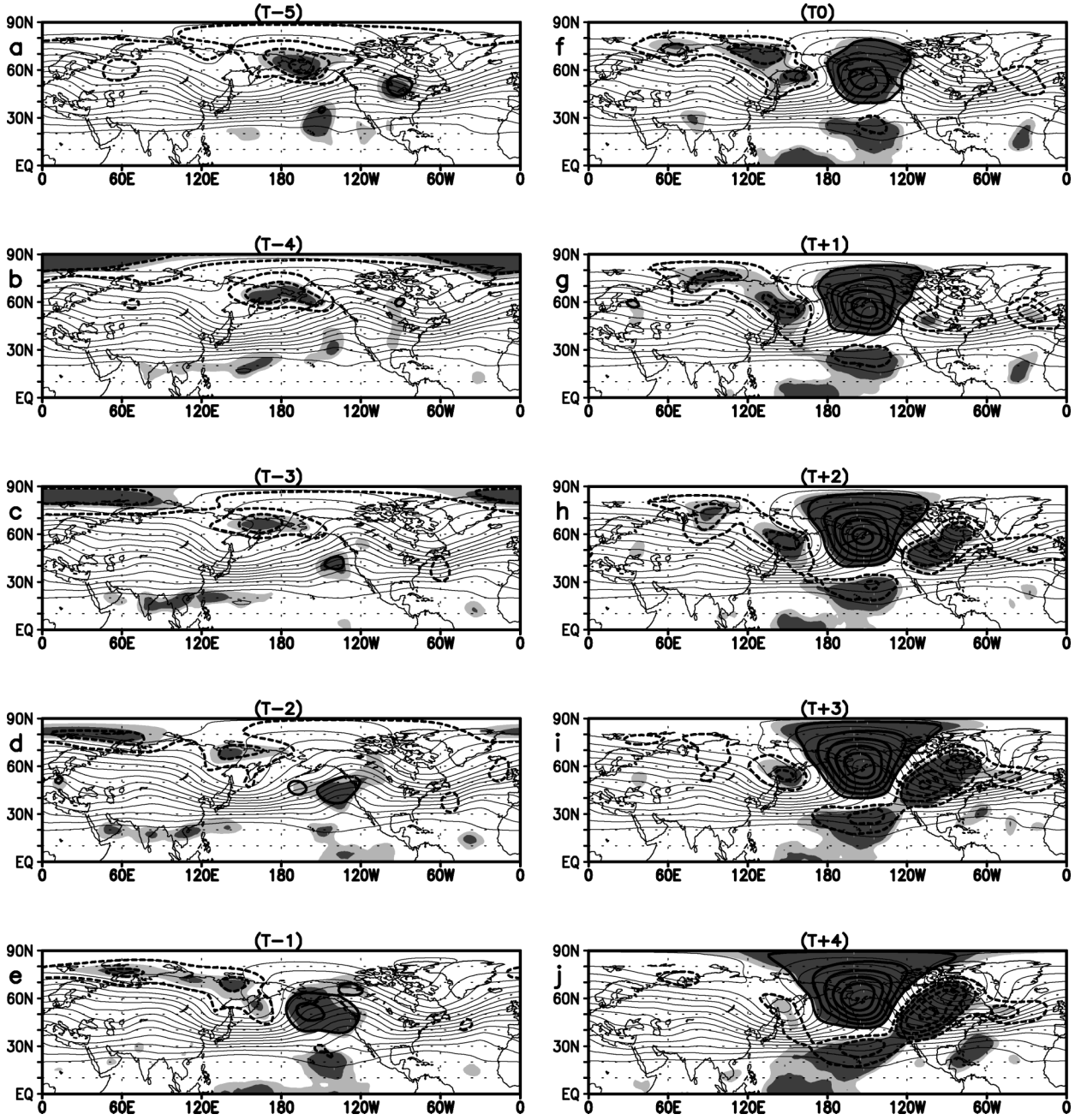

FIG. 3. Composite 500-hPa geopotential height and anomalies shown as a function of the onset time defined as T0. The 500-hPa geopotential heights are given in thin solid lines with a contour interval of 60 m. Thick solid (dashed) contours represent positive (negative) 500-hPa geopotential height anomalies. Contour interval for positive (negative) anomalies is 50 (25) m. Dark (light) shading denotes statistical significance for 500-hPa geopotential height anomalies at the 99% (95%) level: (a) T − 5, (b) T − 4, (c) T − 3, (d) T − 2, (e) T − 1, (f) T0, (g) T + 1, (h) T + 2, (i) T + 3, and (j) T + 4.

(see Rosen et al. 1979; Trenberth and Guillemot 1995), respectively. Consistent with the pronounced upper-level trough over the North Pacific (Figs. 3a,b) negative SLP anomalies occupy the key region roughly 5 days before onset (Figs. 5a,b). Two separate positive SLP anomalies appear to merge as the main positive SLP anomaly drifts northward into the key region by the onset (Figs. 5b–e). Just prior to blocking onset a strengthening negative SLP anomaly is found upstream over the northwestern Pacific (Figs. 5d,e). One can clearly see the equivalent barotropic, or warm core structure, of the blocking events with the large area of positive SLP anomalies beneath the pronounced blocking ridge (Figs. 3f–j, and 5f–j). This warm core structure

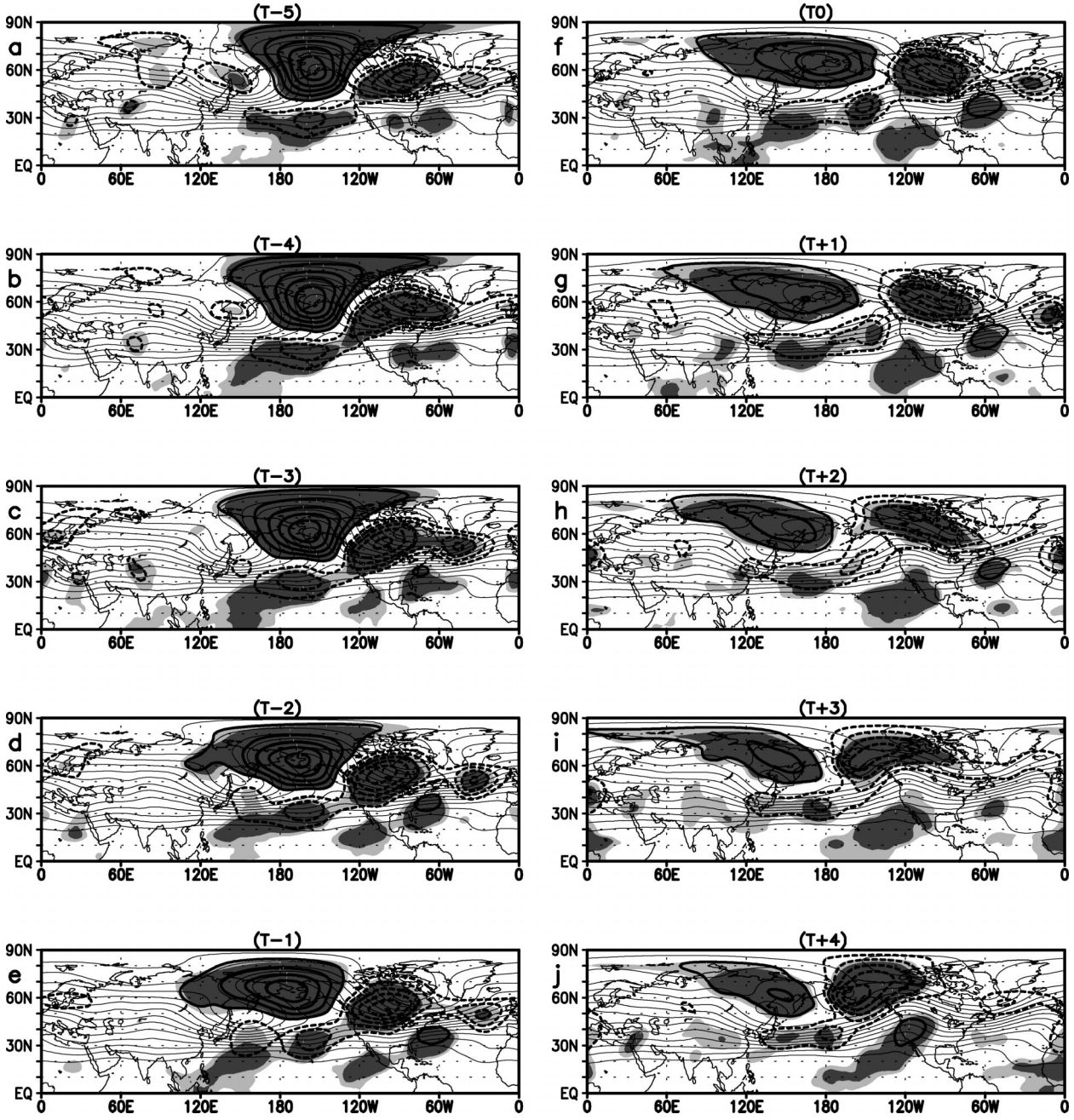

FIG. 4. Same as Fig. 3 but for end time.

is characteristic of mid- to high-latitude blocks (Dole 1986a). Pelly and Hoskins (2003a,b) recently developed a new atmospheric blocking index, based upon potential vorticity and potential temperature, which implicitly looks for a warm potential temperature anomaly on the dynamic tropopause (Morgan and Nielsen-Gammon 1998) at high latitudes, indicative of atmospheric blocks.

The ridging over Alaska extends southeastward over central North America with a secondary area of pronounced ridging off the U.S. southeast coast by T + 4 (Fig. 5j). Also evident is the equatorward displacement of the Pacific storm track (Figs. 5h–j) to the south of the blocking anticyclone. Pronounced southwesterly moisture transport, emanating from the subtropical North Pacific and converging into the U.S. southwest is clearly evident (Figs. 5h–j). Previous studies have shown that this ''Pineapple Express,'' so named because of the enhanced moisture transport across the Hawaiian Islands, can lead to heavy precipitation along the U.S.

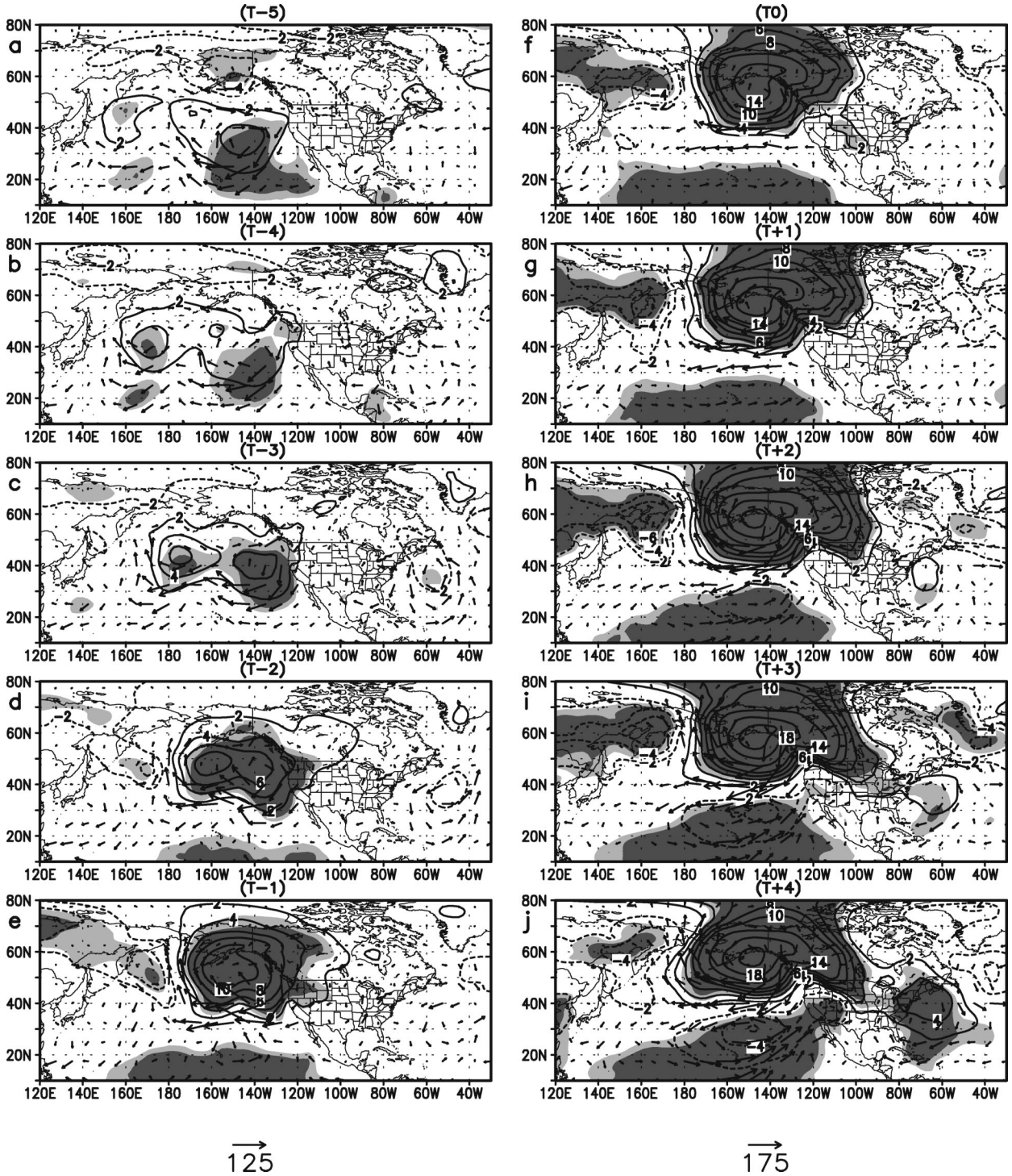

FIG. 5. As in Fig. 3 except for SLP and vertically integrated moisture transport anomalies (kg m^{-1} s^{-1}). Contour interval for SLP is 2 hPa to a magnitude of 10 hPa, with every 4 hPa for larger magnitudes. Negative values are dashed. Dark (light) shading denotes statistical significance at the 99% (95%) level for SLP anomalies.

west coast (Ely et al. 1994; Lackmann and Gyakum 1999; Higgins et al. 2000a). Additionally, at T + 3 and T + 4 (Figs. 5i,j) there is evidence of anomalous moisture convergence into the Ohio Valley and the southeast, owing to the enhanced ridging off the U.S. southeast coast.

The decay phase of the blocking events is accompanied by a deepening negative SLP anomaly in the

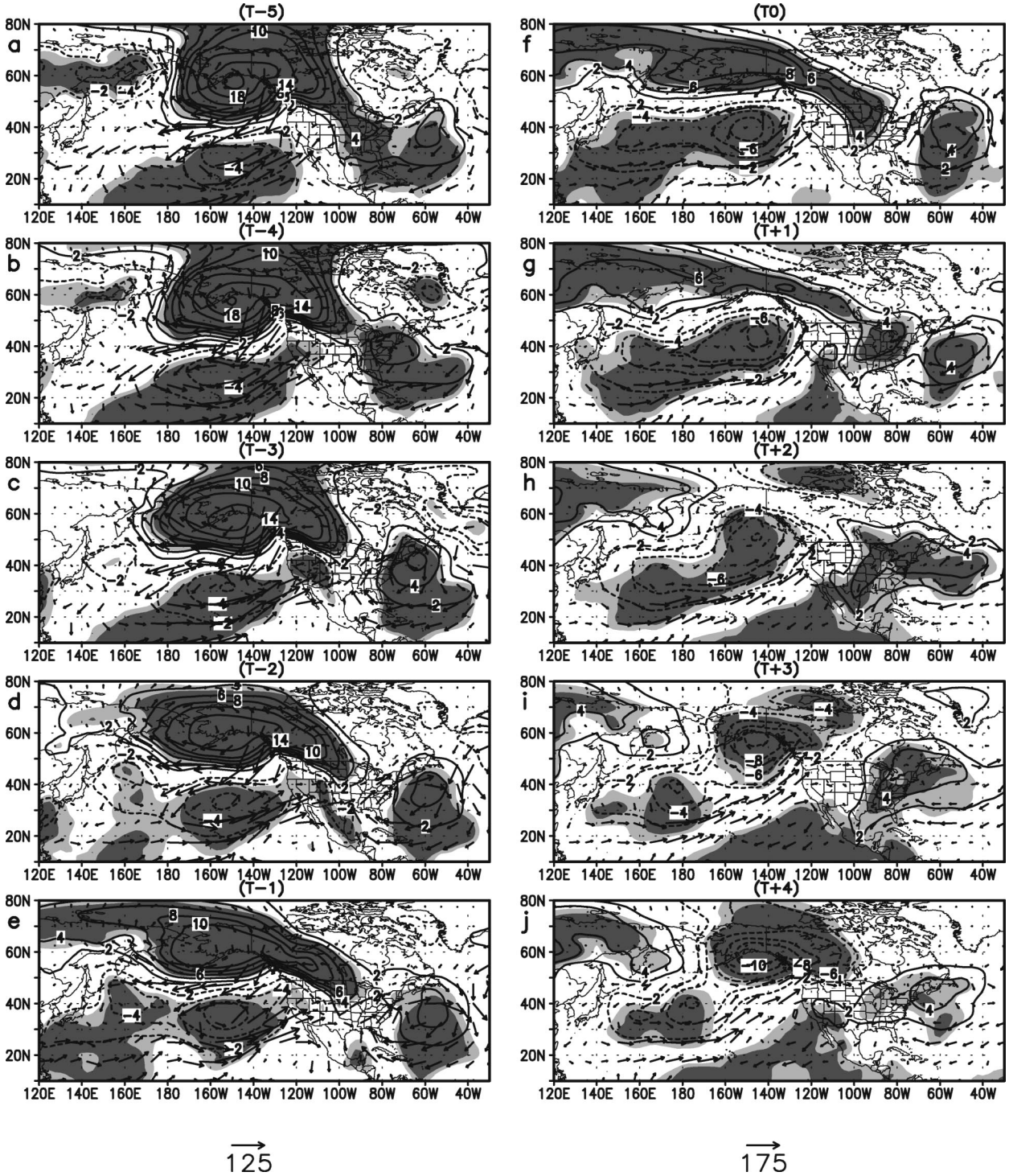

FIG. 6. As in Fig. 4 except for SLP and vertically integrated moisture transport anomalies (kg m^{-1} s^{-1}). Contour interval for SLP is 2 hPa to a magnitude of 10 hPa, with every 4 hPa for larger magnitudes. Negative values are dashed. Dark (light) shading denotes statistical significance at the 99% (95%) level for SLP anomalies.

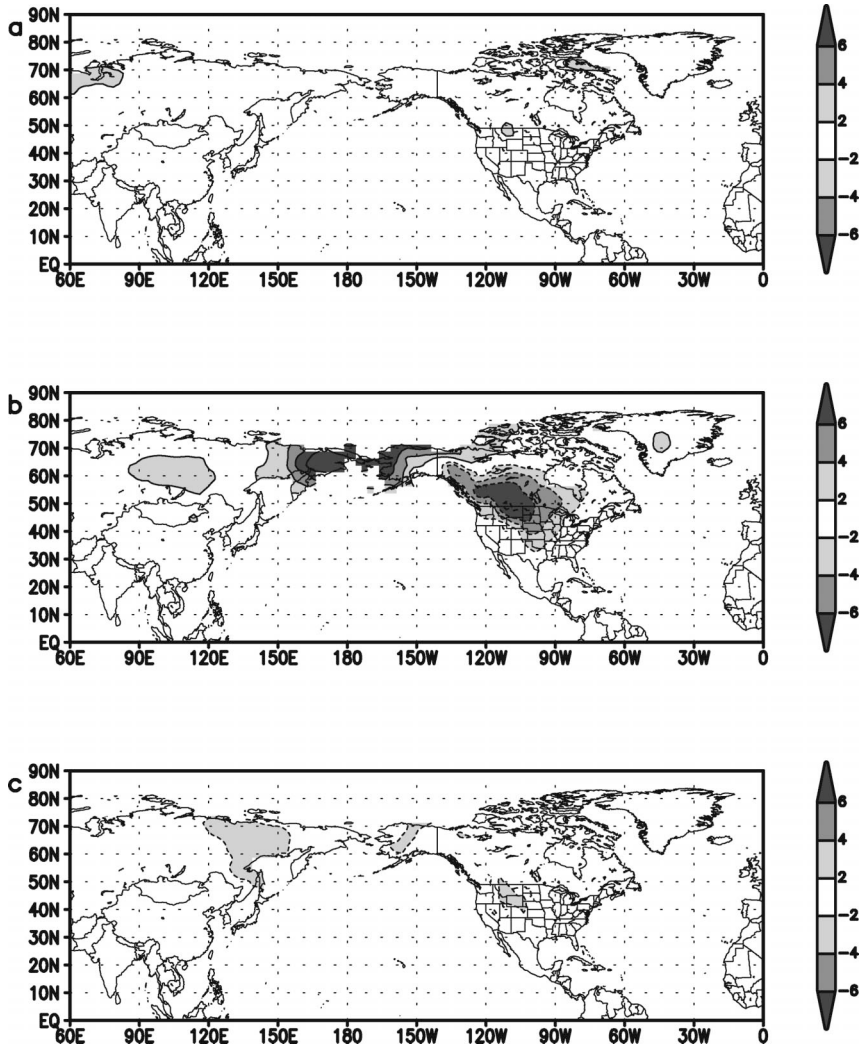

FIG. 7. Composite daily mean surface temperature anomalies (°C), shaded according to the given scale. Solid (dashed) contours represent positive (negative) anomalies. (a) Time average over 11 day period prior to blocking onset. (b) Time average over duration of blocking events. (c) Time average over 11-day period subsequent to blocking termination.

region of the Gulf of Alaska (Figs. 6f–j). Also evident is a splitting of the main positive SLP anomaly, with one region retrograding westward toward the northwest Pacific, the other spreading southeastward over the central United States (Figs. 6d–g) resembling a cold surge anticyclone (Schultz et al. 1998). Colucci and Davenport (1987) examined events of rapid surface anticyclogenesis over western North America and found that the majority of the events were part of a downstream development involving upstream explosive cyclogenesis in the Pacific Ocean. Downstream of the explosive cyclogenesis, a 500-hPa ridge intensifies and is often associated with cold air outbreaks over North America. One can see the enhanced ridging along the west coast of North America (Figs. 4g–j) in association with the deepening cyclone in the Gulf of Alaska (Figs. 6f–j). Several days after the decay of the block the vertically integrated moisture transport returns to the Pacific Northwest as the Pacific strom track shifts to its more poleward trajectory (Figs. 6h–j).

c. Mean daily surface temperature anomalies

Surface temperature changes during the Alaskan blocking episodes are highlighted in Fig. 7. Similar to the 500-hPa geopotential height, SLP, and vertically integrated moisture transport anomalies, the mean daily surface temperature anomalies were calculated by removing the mean plus the first four harmonics of the 22-yr (1979–2000) mean annual cycle. We consider three separate time averages: (i) the 11-day period prior to blocking, (ii) the time period during the blocking event, and (iii) the 11-day period following the blocking event. Eleven-day periods are chosen because this is

approximately equal to the average duration of the Alaskan blocking events (see Table 1). A very pronounced surface temperature signal is present during the Alaskan blocking regime (Fig. 7b) as compared to the periods before and after (Figs. 7a,c).

During the Alaskan blocking regime, negative surface temperature anomalies extend southeastward from northwestern Canada to the southern plains of the United States. Referring back to Figs. 5f–j, the near-surface wind field is northwesterly and persistent over this region. To the northwest over western Alaska and Siberia, where southerly and southeasterly flow dominates near the surface (Figs. 5f–j), positive surface temperature anomalies prevail (Fig. 7b).

5. Temperature and precipitation distributions during Alaskan blocking

In this section we examine the linkage between extremes of surface temperature and precipitation and the occurrence of Alaskan blocking. Specifically, we compare the statistical distributions of daily mean surface temperature and precipitation during the Alaskan blocking regime with the climatological December–March 1979–2000 distributions. The aim is to determine if extremes of surface temperature and precipitation are more likely to occur during the Alaskan blocking regime.

a. Surface temperature distribution

We first calculate the daily surface temperature anomalies by removing a smooth annual cycle defined as the mean daily values for each day of the year based upon the 22-yr period from 1979 to 2000. We next consider all days belonging to DJFMs and rank the daily anomalies to calculate the upper and lower terciles. Removing the seasonal cycle and considering anomalies ensures that cold (warm) extremes are not biased to occur in December (March). By definition, each tercile will contain one-third of the daily anomalies. The set of days belonging to Alaskan blocking events represents a subset of all 1979–2000 DJFM days, which we will refer to as Alaskan blocking days. Finally, for all Alaskan blocking days we calculate the number of days with daily mean surface temperature anomalies in each of the three climatological DJFM terciles.

We noted that negative or cold surface temperature anomalies were pronounced during Alaskan blocking, extending from northwestern Canada to the southern plains of the United States (Fig. 7b). The percentage of days during Alaskan blocking with daily mean surface temperature anomalies in the lower tercile of the distribution is shown in Fig. 8a. A spatial pattern similar to that in Fig. 7b is evident. In the region extending from northern British Columbia southeastward to the northern plains of the United States over 70% of the Alaskan blocking days possess daily mean surface temperature anomalies in the lower tercile of the distribution. The region encompassing 50% of the days extends from the Yukon southeastward to northern Texas indicating a significant shift in the daily mean surface temperature distribution during Alaskan blocking toward colder temperatures.

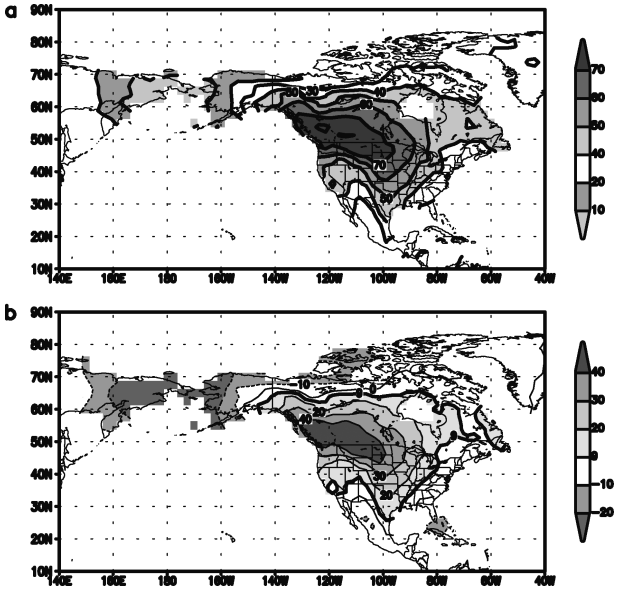

FIG. 8. (a) Percentage of Alaskan blocking days with daily mean surface temperature anomalies in the lower tercile of the 1979–2000 DJFM daily mean surface temperature anomaly distribution. (b) Percentage difference found as the percentage in (a) minus the expected number of 33.3%. Solid (dashed) contours denote positive (negative) values. The thick solid line in (b) denotes the 95% confidence threshold based upon a binomial test (see text).

This shift in the daily mean surface temperature distribution is clearly demonstrated in Fig. 8b, in which the expected value in the lower tercile of 33.3% is subtracted from Fig. 8a. During the Alaskan blocking regime the probabilities of daily mean surface temperatures in each tercile are not equal. In the region extending from the Yukon southeastward to northern Texas there is an increased likelihood of daily mean surface temperatures in the lower tercile.

To determine the local statistical significance of the departures from 33.3% (random chance) we can apply a simple binomial test (Wilks 1995). The relevant parameters are n, the sample size, and p, the expected probability of a given tercile. To attain the 95% confidence threshold, assuming a one-sided test, the actual number of cases in a given tercile must exceed E + (1.65 × sd), where E is the expected number given by np and sd is the standard deviation given by npq, where q is $(1 - p)$. Owing to the serial dependence or persistence of surface temperature we define an effective sample size n', which is smaller than n. Following Wilks (1995), we define the effective sample size (n') as

$$n' \cong n\left(\frac{1 - \rho_1}{1 + \rho_1}\right), \tag{1}$$

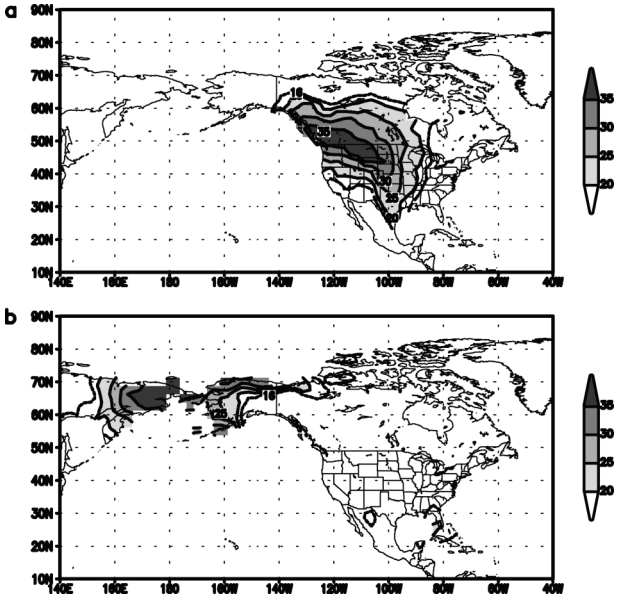

FIG. 9. (a) Percentage of Alaskan blocking days with daily mean surface temperature anomalies less than the 10th percentile of the climatological DJFM distribution. (b) Percentage of Alaskan blocking days with daily mean surface temperature anomalies greater than the 90th percentile of the climatological DJFM distribution. The dashed line in both panels denotes the 95% confidence threshold based upon a binomial test.

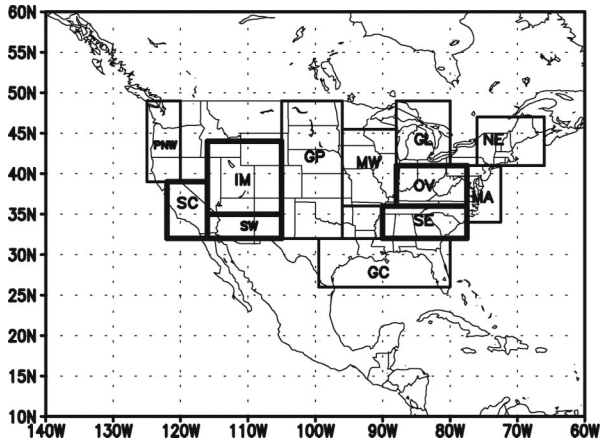

FIG. 10. Rectangular and square boxes depict geographical areas where the area-averaged precipitation is calculated. Areas outlined in thick black represent locations with extreme precipitation events, which are discussed in the text: PNW, Pacific Northwest; SC, southern California; SW, Southwest; IM, Intermountain West; GP, Great Plains; MW, Midwest; GL, Great Lakes; OV, Ohio Valley; SE, Southeast; GC, Gulf coast; MA, mid-Atlantic; and NE, Northeast.

where ρ_1 is the lag-1 autocorrelation coefficient. For surface temperature the lag-1 autocorrelation coefficient is taken as 0.7 (Van den Dool et al. 1986; Barnston 1993). Performing the calculations we find that the 95% confidence threshold is 42%, representing roughly a 9% percentage difference (42% − 33.3%) in Fig. 8b. Hence much of the negative surface temperature anomalies extending from northern Canada to the southern plains of the United States are statistically significant.

The shift toward colder (warmer) daily mean surface temperatures during Alaskan blocking (Fig. 8) is also accompanied by a shift in the tails of the daily mean surface temperature distribution toward more extreme cold (warm) days. The fraction of Alaskan blocking days with daily mean surface temperature anomalies below the 10th percentile (defined as extreme cold) of the DJFM 1979–2000 climatological distribution is shown in Fig. 9a. Recall that the expected value is 10%. The spatial pattern is similar to that of Fig. 8. Extreme cold days during Alaskan blocking events are found in the region stretching from British Columbia southeastward to the central plains of the United States with more than 25% of the days possessing daily mean surface temperature anomalies below the 10th percentile. In this region there is also a reduced variance in surface temperatures (not shown). Over western Alaska the shift toward warmer daily mean surface temperatures (Fig. 8) is also associated with the occurrence of extreme warm days (Fig. 9b) and a reduced variance in surface temperatures (not shown). Applying the binomial test described above, the 95% confidence threshold to conclude that the 10th (90th) percentile classes have more cases than expected is roughly 16%.

b. Precipitation distribution

To examine the relationship between Alaskan blocking and the occurrence of extreme daily precipitation events we use a merged U.S.–Mexico historical daily precipitation dataset, analyzed at a horizontal resolution of 1° and derived from rain gauge measurements (see section 2). We divided the contiguous U.S. landmass into 12 geographical areas, as shown in Fig. 10, for the purposes of calculating area-averaged daily precipitation. These 12 geographical areas capture the major climatic zones of the United States and are the same as those used in the monthly *Climate Diagnostics Bulletin* issued by CPC. From the time series of area-averaged precipitation for each of the 12 geographical regions we considered only those days during the DJFM 1979–2000 period with area-averaged precipitation greater than or equal to 1 mm day^{-1} (measurable precipitation days) and calculated the 90th percentile of the daily area-averaged precipitation. In this study, days with area-averaged precipitation greater than the climatological DJFM 90th percentile are considered to be extreme heavy precipitation days.

Similar to the daily mean surface temperature analysis we consider the set of Alaskan blocking days as a subset of all DJFM days and calculate the number of days with area-averaged precipitation greater than the climatological DJFM 90th percentile. Table 2a summarizes the findings. Three regions in the western half of the contiguous United States, southern California (15.2%), the

TABLE 2. The 90th percentile of area-averaged daily precipitation for a measurable precipitation threshold of (a) 1 and (b) 3 mm day^{-1}. In (a) and (b), the first column refers to a given area over the United States (see Fig. 10): PNW, Pacific Northwest; SC, southern California; SW, Southwest; IM, Intermountain West; GP, Great Plains; MW, Midwest; GL, Great Lakes; OV, Ohio Valley; SE, Southeast; GC, Gulf coast; MA, mid-Atlantic; and NE, Northeast. The second column refers to the number of Alaskan blocking events with at least 1 day with area-averaged precipitation (P) greater than the 90th percentile, the third column to the total number of days with P greater than the 90th percentile, the fourth column to the total number of Alaskan blocking days with measurable precipitation, and the fifth column to the percentage of Alaskan blocking days with P greater than the 90th percentile.

(a)

Threshold (1 mm day^{-1})	No. of events	Total No. of days	Total No. of Alaskan blocking days with $P >= 1$ mm day^{-1}	Percentage of Alaskan blocking days with $P >$ 90th percentile
PNW	13	25	274	9.1
SC	14	25	164	15.2
SW	10	17	101	16.8
IM	15	28	154	18.2
GP	5	6	68	8.8
MW	11	14	157	8.9
GL	15	25	204	12.3
OV	23	34	225	15.1
SE	23	35	248	14.1
GC	14	20	245	8.2
MA	13	16	209	7.7
NE	12	16	177	9.0

(b)

Threshold (3 mm day^{-1})	No. of events	Total No. of days	Total No. of Alaskan blocking days with $P >= 3$ mm day^{-1}	Percentage of Alaskan blocking days with $P >$ 90th percentile
PNW	9	17	193	8.8
SC	9	14	111	12.6
SW	4	10	54	18.5
IM	7	10	48	20.8
GP	1	1	12	8.3
MW	8	8	82	9.8
GL	9	9	76	11.8
OV	15	20	140	14.3
SE	14	21	171	12.3
GC	11	13	136	9.6
MA	6	9	117	7.7
NE	7	9	105	8.6

southwest (16.8%), and the Intermountain West region (18.2%), all have a total number of Alaskan blocking days with area-averaged precipitation above the climatological 90th percentile of at least 15% or greater. Recall that the expected value is 10%. This finding is consistent with the equatorward shift of the North Pacific storm track and area of anomalous vertically integrated moisture transport convergence (Figs. 5h–j) during Alaskan blocking.

If we examine the southern California region in more detail, we can see from the second column of Table 2a that the heavy precipitation days were distributed among 14 Alaskan blocking events. We calculated the time-averaged SLP and vertically integrated moisture transport anomalies, averaged over all 14 Alaskan blocking events associated with at least 1 day of heavy precipitation over southern California (Fig. 11b). For reference, Fig. 11b can be compared with the average for all 37 Alaskan blocking events (Fig. 11a). Alaskan blocking events with heavy precipitation over southern California possess a stronger negative SLP anomaly (i.e., more pronounced storm track) equatorward of the blocking anticyclone when compared to all blocking events. The storm track over the Pacific extends farther eastward to the U.S. west coast and the accompanying vertically integrated moisture transport from the subtropical Pacific is more pronounced.

Over the eastern half of the United States the Ohio Valley (15.1%) and the southeast (14.1%) regions experience a greater percentage of heavy precipitation days during Alaskan blocking. A total of 23 Alaskan blocking events are associated with at least 1 day of heavy precipitation over the Ohio Valley region (see Table 2a). Figure 11c shows the time-averaged SLP and vertically integrated moisture transport anomalies, averaged over all 23 events. When compared with the plot for all Alaskan blocking events (Fig. 11a), the Alaskan blocking events with heavy precipitation days over the Ohio Valley are associated with stronger surface ridging off the U.S. southeast coast (Fig. 11c). This enhanced ridging leads to a more pronounced southerly vertically integrated moisture transport into the Southeast and the Ohio Valley from the Gulf of Mexico. This region lies downstream of a large-scale 500-hPa trough (Figs. 3

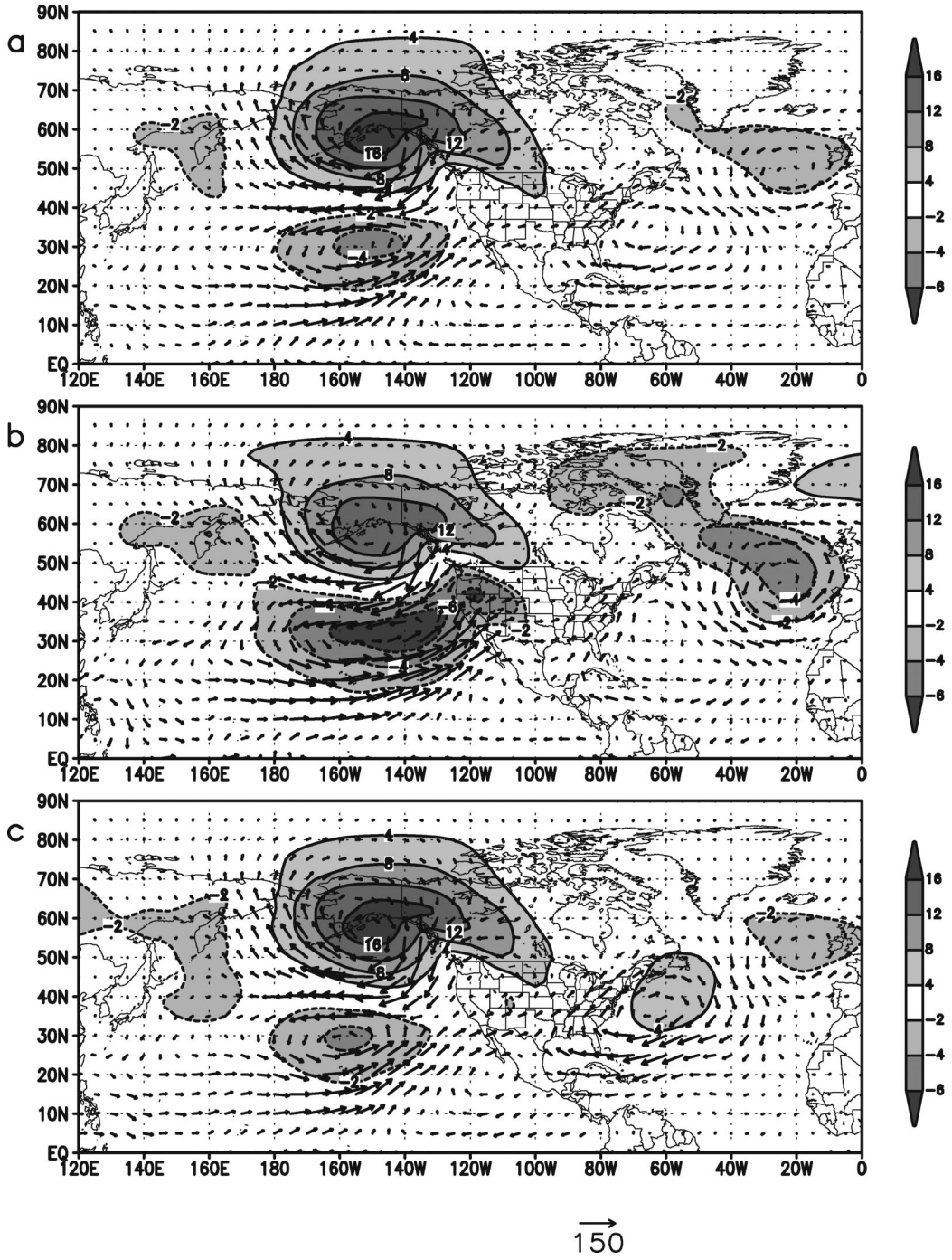

FIG. 11. Time-averaged SLP and vertically integrated moisture transport anomalies (kg m^{-1} s^{-1}) over (a) duration of all 37 Alaskan blocking events, (b) duration of 14 Alaskan blocking events associated with heavy precipitation over southern California, and (c) duration of 23 Alaskan blocking events associated with heavy precipitation over the Ohio Valley. The contour interval for SLP is 2 hPa with shading as indicated and negative values dashed.

and 4). It is not surprising that 18 of the 23 Alaskan blocking events with at least 1 day of heavy precipitation over the Ohio Valley also have at least 1 day of heavy precipitation over the Southeast.

When the area-averaged precipitation threshold is raised to 3 mm day^{-1} (Table 2b), the spatial patterns are similar indicating that the analysis is not sensitive to the choice of precipitation threshold.

6. Summary and conclusions

This study examined the linkage between low-frequency atmospheric variability and weather extremes. Using a threshold crossing procedure applied to the 500-hPa geopotential height field we identified 37 events of atmospheric blocking over the Alaskan region of the northeast Pacific, referred to as Alaskan blocking, during the boreal winter season from 1979 to 2000. The blocking events had durations ranging from 8 to 25 days, with a mean duration of 11.3 days. A total of 417 out of the 2668 (December–March 1979–2000) days, or 15.6%, belonged to an Alaskan blocking event.

The number of blocked days over the Alaskan region was found to be sensitive to the phase of the ENSO cycle. A reduced (increased) number of blocked days was found during El Niño (La Niña/neutral) conditions. The average number of blocked days during El Niño winters was 12, compared with 31.2 and 27 for neutral and La Niña winters. Despite the small sample size of El Niño winters, the difference in the mean number of blocked days between El Niño and neutral winters was found to be statistically significant. The analysis was not sensitive to the key point of 62.5°N, 162.5°W as the eight surrounding grid points also showed a preference for a reduced number of blocked days during El Niño winters as compared to either neutral or La Niña winters.

An examination of the composite structure and temporal evolution of the Alaskan blocking events revealed the presence of a pronounced trough or negative 500-hPa geopotential height anomaly over the Alaskan region prior to onset. The trough along the Asian coast in the North Pacific deepens just prior to onset. The high-amplitude ridging, which forms the Alaskan block, appears to retrograde from the west coast of North America into the key region. The mature block is associated with an equatorward trough in the subtropical North Pacific and pronounced troughing downstream over North America. The Alaskan blocking decay is rapid and involves the retrograding of the main positive and negative anomaly centers northwestward toward the northwest Pacific.

The SLP and vertically integrated moisture transport analyses revealed the strong equivalent barotropic nature, or warm core structure, of the blocks. Also clearly evident was the equatorward displacement of the Pacific storm track to the south of the blocking anticyclone. Anomalous moisture transport is found over the U.S. southwest and the Ohio Valley and southeast regions.

An examination of the linkage between extremes of daily mean surface temperature and the occurrence of Alaskan blocking revealed a significant shift in the daily mean surface temperature distribution toward colder temperatures in the region extending from the Yukon southeastward to the southern plains of the United States, associated with a reduced surface temperature variance. Similarly, over extreme western Alaska there was a shift in the daily mean surface temperature distribution toward warmer temperatures. The shift toward colder (warmer) daily mean surface temperatures during Alaskan blocking is also accompanied by a shift in the tails of the distribution toward more extreme cold (warm) days in these two regions.

A similar analysis of extremes in daily precipitation revealed that the regions of southern California, the Southwest, and the Intermountain West all possess a higher frequency of heavy precipitation days when compared with the long-term DJFM climatology. Alaskan blocking events with heavy precipitation over southern California possess a stronger negative SLP anomaly, or more enhanced storm track, equatorward of the blocking anticyclone when compared to all blocking events. The storm track over the Pacific also extends farther eastward to the U.S. west coast and the accompanying vertically integrated moisture transport from the subtropical Pacific is more pronounced.

Over the eastern half of the United States, the Ohio Valley and the southeast regions experience a greater percentage of heavy precipitation days during Alaskan blocking. When compared with the plot for all Alaskan blocking events, the surface ridging off the U.S. southeast coast is more pronounced. This ridging leads to enhanced southerly vertically integrated moisture transport into the Southeast and Ohio Valley regions from the Gulf of Mexico.

This study addressed the large-scale aspects of the atmospheric blocking–surface weather relationship in an effort to provide guidance to climate forecasters at CPC, who require information for large-scale areas, to produce the extended-range (6–10- and 8–14-day, and U.S. Hazards Assessment) outlooks. For the 6–10- and 8–14-day outlooks, forecasters attempt to make a probabilistic forecast for surface temperature and precipitation, expressing the deviation from the climatological forecast of 33.3% for each tercile category. Given an Alaskan blocking scenario forecasted with the model guidance products, results from Fig. 8 can provide the forecaster with information on how to alter the probabilities of the given surface temperature tercile categories. The U.S. Hazards Assessment is intended to provide emergency managers, planners, forecasters, and the public with advance notice of potential hazards related to climate, weather, and hydrological events. The results from Fig. 9 and Table 2 clearly demonstrate the strong relationship between Alaskan blocking and extreme cold and heavy precipitation. The regions chosen in Fig. 10 are ideally suited for the U.S. Hazards Assessment as they summarize the atmospheric blocking and heavy precipitation relationships on the larger scales.

Finally, as discussed in the introduction, the longitudinal extent of the atmospheric blocking maximum over the North Pacific is broad. In this study we focused upon the region of Alaska, one of the preferred regions for atmospheric blocking in the North Pacific. There are other regions over the North Pacific that are preferred regions for atmospheric blocking. The downstream

weather impacts over North America depend largely upon the location of the blocking anticyclone and downstream trough. In future work we plan to examine the downstream weather impacts associated with atmospheric blocking in other regions of the North Pacific.

Acknowledgments. Financial support for this study came from a National Research Council Research Associateship Award. We would like to thank Dr. Pingping Xie and Dr. Hyun-Kyung Kim for help in processing the global surface temperature dataset. Dr. Wei Shi kindly provided the U.S.–Mexico merged historical daily precipitation analysis. We greatly appreciate the comments and suggestions of Dr. Huug Van den Dool, Dr. Martin Hoerling, Mr. John Janowiak, and those of two anonymous reviewers.

REFERENCES

Anderson, J. L., 1993: The climatology of blocking in a numerical forecast model. *J. Climate,* **6,** 1041–1056.

Barnston, A. G., 1993: *Atlas of Frequency Distribution, Autocorrelation and Cross-Correlation of Daily Temperature and Precipitation at Stations in the U.S., 1948–1991. NOAA Atlas 11,* 440 pp. [Available from Climate Prediction Center, World Weather Bldg., Rm. 605, 5200 Auth Rd., Camp Springs, MD 20746.]

Black, R. X., 1997: Deducing anomalous wave source regions during the life cycles of persistent flow anomalies. *J. Atmos. Sci.,* **54,** 895–907.

——, and K. J. Evans, 1998: The statistics of horizontal structure of anomalous weather regimes in the Community Climate Model. *Mon. Wea. Rev.,* **126,** 841–859.

Chen, W. Y., and H. M. Van den Dool, 1995: Low-frequency anomalies in the NMC MRF model and reality. *J. Climate,* **8,** 1369–1385.

——, and ——, 1997: Asymmetric impact of tropical SST anomalies on atmospheric internal variability over the North Pacific. *J. Atmos. Sci.,* **54,** 725–740.

——, and ——, 1999: Significant change of extratropical natural variability and potential predictability associated with the El Nino/Southern Oscillation. *Tellus,* **51A,** 790–802.

Colucci, S. J., and J. C. Davenport, 1987: Rapid surface anticyclogenesis: Synoptic climatology and attendant large-scale circulation changes. *Mon. Wea. Rev.,* **115,** 822–836.

Compo, G. P., P. D. Sardeshmukh, and C. Penland, 2001: Changes of subseasonal variability associated with El Niño. *J. Climate,* **14,** 3356–3374.

D'Andrea, F., and Coauthors, 1998: Northern Hemisphere atmospheric blocking as simulated by 15 atmospheric general circulation models in the period 1979–1988. *Climate Dyn.,* **14,** 385–407.

Dole, R. M., 1986a: Persistent anomalies of the extratropical Northern Hemisphere wintertime circulation: Structure. *Mon. Wea. Rev.,* **114,** 178–207.

——, 1986b: The life cycles of persistent anomalies and blocking over the North Pacific. *Advances in Geophysics,* Vol. 29, Academic Press, 31–69.

——, 1989: Life cycles of persistent anomalies. Part I: Evolution of 500 mb height fields. *Mon. Wea. Rev.,* **117,** 177–211.

——, and N. D. Gordon, 1983: Persistent anomalies of the extratropical Northern Hemisphere wintertime circulation: Geographical distribution and regional persistence characteristics. *Mon. Wea. Rev.,* **111,** 1567–1586.

Duchon, C. E., 1979: Lanczos filtering in one and two dimensions. *J. Appl. Meteor.,* **18,** 1016–1022.

Elliott, R. D., and T. B. Smith, 1949: A study of the effects of large blocking highs on the general circulation in the Northern Hemisphere westerlies. *J. Meteor.,* **6,** 67–85.

Ely, L. L., Y. Enzel, and D. R. Cayan, 1994: Anomalous North Pacific atmospheric circulation and large winter floods in the southwestern United States. *J. Climate,* **7,** 977–987.

Higgins, R. W., and S. D. Schubert, 1994: Simulated life cycles of persistent anticyclonic anomalies over the North Pacific: Role of synoptic-scale eddies. *J. Atmos. Sci.,* **51,** 3238–3260.

——, and ——, 1996: Simulations of persistent North Pacific circulation anomalies and interhemispheric teleconnections. *J. Atmos. Sci.,* **53,** 188–207.

——, and K. C. Mo, 1997: Persistent North Pacific circulation anomalies and the tropical intraseasonal oscillation. *J. Climate,* **10,** 223–244.

——, J.-K. E. Schemm, W. Shi, and A. Leetmaa, 2000a: Extreme precipitation events in the western United States related to tropical forcing. *J. Climate,* **13,** 793–820.

——, W. Shi, E. Yarosh, and R. Joyce, 2000b: *Improved United States Precipitation Quality Control System and Analysis. NCEP/Climate Prediction Center Atlas 7,* U.S. Department of Commerce, 40 pp. [Available online at http://www.cpc.ncep.noaa.gov/research_papers/ncep_cpc_atlas/7/index.html.]

——, A. Leetmaa, and V. E. Kousky, 2002: Relationships between climate variability and winter temperature extremes in the United States. *J. Climate,* **15,** 1555–1572.

Hogg, R. V., and E. A. Tanis, 1988: *Probability and Statistical Inference*. MacMillan, 658 pp.

Kalkstein, L. S., P. F. Jamason, J. S. Greene, J. Libby, and L. Robinson, 1996: The Philadelphia hot weather-health watch/warning system: Development and application, summer 1995. *Bull. Amer. Meteor. Soc.,* **77,** 1519–1528.

Kalnay, E., and Coauthors, 1996: The NCEP/NCAR 40-Year Reanalysis Project. *Bull. Amer. Meteor. Soc.,* **77,** 437–471.

Karl, T. R., and R. W. Knight, 1997: The 1995 Chicago heat wave: How likely is a recurrence? *Bull. Amer. Meteor. Soc.,* **78,** 1107–1119.

Kistler, R., W. Collins, S. Saha, G. White, and J. Woollen, 2001: The NCEP–NCAR 50-Year Reanalysis: Monthly means CD-ROM and documentation. *Bull. Amer. Meteor. Soc.,* **82,** 247–268.

Lackmann, G. M., and J. R. Gyakum, 1999: Heavy cold-season precipitation in the northwestern United States: Synoptic climatology and an analysis of the flood of 17–18 January 1986. *Wea. Forecasting,* **14,** 687–700.

Lau, N.-C., 1997: Interactions between global SST anomalies and the midlatitude atmospheric circulation. *Bull. Amer. Meteor. Soc.,* **78,** 21–33.

Mo, K. C., and H.-M. H. Juang, 2003: Relationships between soil moisture and summer precipitation over the Great Plains and the Southwest. *J. Geophys. Res.,* **108,** 8610, doi:10.1029/2002JD002952.

——, and E. H. Berbery, 2004: Low-level jets and the summer precipitation regimes over North America. *J. Geophys. Res.,* **109,** D06117, doi:10.1029/2003JD004106.

——, J. Nogues Peagle, and R. W. Higgins, 1997: Atmospheric processes associated with summer floods and droughts in the central United States. *J. Climate,* **10,** 3028–3046.

Morgan, M. C., and J. W. Nielsen-Gammon, 1998: Using tropopause maps to diagnose midlatitude weather systems. *Mon. Wea. Rev.,* **126,** 2555–2579.

Mullen, S. L., 1989: Model experiments on the impact of Pacific sea surface temperature anomalies on blocking frequency. *J. Climate,* **2,** 997–1013.

Nakamura, H., and J. M. Wallace, 1990: Observed changes in baroclinic wave activity during the life cycles of low-frequency circulation anomalies. *J. Atmos. Sci.,* **47,** 1100–1116.

Pelly, J. L., and B. J. Hoskins, 2003a: A new perspective on blocking. *J. Atmos. Sci.,* **60,** 743–755.

——, and ——, 2003b: How well does the ECMWF Ensemble Prediction System predict blocking? *Quart. J. Roy. Meteor. Soc.,* **129,** 1683–1702.

Renwick, J. A., 1998: ENSO-related variability in the frequency of South Pacific blocking. *Mon. Wea. Rev.,* **126,** 3117–3123.

——, and J. M. Wallace, 1996: Relationships between North Pacific wintertime blocking, El Niño, and the PNA pattern. *Mon. Wea. Rev.,* **124,** 2071–2076.

Rex, D. F., 1950a: Blocking action in the middle troposphere and its effect upon regional climate. I. An aerological study of blocking action. *Tellus,* **2,** 196–211.

——, 1950b: Blocking action in the middle troposphere and its effect upon regional climate. II. The climatology of blocking action. *Tellus,* **2,** 275–301.

Robertson, A. W., and M. Ghil, 1999: Large-scale weather regimes and local climate over the western United States. *J. Climate,* **12,** 1796–1813.

Rosen, R. D., D. A. Salstein, and J. P. Peixoto, 1979: Streamfunction analysis of interannual variability in large-scale water vapor flux. *Mon. Wea. Rev.,* **107,** 1682–1684.

Schultz, D. M., W. E. Bracken, and L. F. Bosart, 1998: Planetary- and synoptic-scale signatures associated with Central American cold surges. *Mon. Wea. Rev.,* **126,** 5–27.

Stoss, L. A., and S. L. Mullen, 1995: The dependence of short-range 500-mb height forecasts on the initial flow regime. *Wea. Forecasting,* **10,** 353–368.

Tibaldi, S., and F. Molteni, 1990: On the operational predictability of blocking. *Tellus,* **42A,** 343–365.

——, E. Tosi, A. Navarra, and L. Pedulli, 1994: Northern and Southern Hemisphere seasonal variability of blocking frequency and predictability. *Mon. Wea. Rev.,* **122,** 1971–2003.

Trenberth, K. E., and C. J. Guillemot, 1995: Evaluation of the global atmospheric moisture budget as seen from analyses. *J. Climate,* **8,** 2255–2280.

——, and ——, 1996: Physical processes involved in the 1988 drought and 1993 floods in North America. *J. Climate,* **9,** 1288–1298.

Van den Dool, H. M., W. H. Klein, and J. E. Walsh, 1986: The geographical distribution and seasonality of persistence in monthly mean air temperature over the United States. *Mon. Wea. Rev.,* **114,** 546–560.

Watson, J. S., and S. J. Colucci, 2002: Evaluation of ensemble predictions of blocking in the NCEP Global Spectral Model. *Mon. Wea. Rev.,* **130,** 3008–3021.

Wilks, D. S., 1995: *Statistical Methods in the Atmospheric Sciences*. Academic Press, 467 pp.

Xie, P., B. Rudolf, U. Schneider, and P. A. Arkin, 1996: Gauge-based monthly analysis of global land precipitation from 1971–1994. *J. Geophys. Res.,* **101** (D14), 19 023–19 034.